CONFIDENTIAL

Copy 327
RM L56E04

NACA RM L56E04

NACA

CASE FILE
COPY

RESEARCH MEMORANDUM

COMPARISON OF THE MINIMUM DRAG OF TWO VERSIONS OF A MODIFIED DELTA-WING FIGHTER AS OBTAINED FROM FLIGHT TESTS OF ROCKET-BOOSTED MODELS AND EQUIVALENT BODIES BETWEEN MACH NUMBERS OF 0.80 AND 1.64

By Earl C. Hastings, Jr., and Grady L. Mitcham

Langley Aeronautical Laboratory
Langley Field, Va.

CLASSIFICATION CHANGED TO UNCLASSIFIED
AUTHORITY: NASA TECHNICAL PUBLICATIONS ANNOUNCEMENTS NO. 9
EFFECTIVE DATE: SEPT. 1, 1959
NIL

CLASSIFIED DOCUMENT

This material contains information affecting the National Defense of the United States within the meaning of the espionage laws, Title 18, U.S.C., Secs. 793 and 794, the transmission or revelation of which in any manner to an unauthorized person is prohibited by law.

NATIONAL ADVISORY COMMITTEE
FOR AERONAUTICS

WASHINGTON

September 24, 1956

CONFIDENTIAL

NATIONAL ADVISORY COMMITTEE FOR AERONAUTICS

RESEARCH MEMORANDUM

COMPARISON OF THE MINIMUM DRAG OF TWO VERSIONS OF A MODIFIED DELTA-WING FIGHTER AS OBTAINED FROM FLIGHT TESTS OF ROCKET-BOOSTED MODELS AND EQUIVALENT BODIES BETWEEN MACH NUMBERS OF 0.80 AND 1.64

By Earl C. Hastings, Jr., and Grady L. Mitcham

SUMMARY

An investigation has been conducted to determine the reduction in minimum drag that could be obtained at supersonic speeds by redesigning the fuselage and reducing the wing and tail thickness of a modified delta-wing fighter-type airplane. This investigation was conducted with rocket-boosted models and equivalent bodies of revolution.

The results of the tests indicate that, at a Mach number of 1.00, the modifications result in a reduction in external drag coefficient from 0.035 to a value of 0.022. At a Mach number of 1.35, the external drag coefficient is reduced from 0.038 to 0.024. The average drag reduction between these Mach numbers is about 0.013. The drag-rise Mach number is delayed from 0.93 to 0.97.

INTRODUCTION

The National Advisory Committee for Aeronautics is conducting a flight investigation by use of rocket-boosted models of a modified delta-wing fighter airplane to evaluate the drag at transonic and supersonic speeds. The results from the first phase of this investigation are presented in reference 1.

In reference 1 it was suggested that a large reduction in drag could be accomplished at supersonic speeds by decreasing the wing fillet thickness, modifying the rear fuselage lines, and reducing the wing and vertical-tail thickness. As a result of these suggestions, it was decided that the test program should be extended to determine the magnitude of this reduction. Evaluation tests of various proposed modifications were made by free-flight tests of small equivalent bodies of

revolution which were designed according to the transonic-area-rule concept and provided a simple and inexpensive means of estimating the zero-lift pressure drag and drag rise of thin, low-aspect-ratio wing-body combinations. The revised design was then tested by use of large-scale rocket-boosted models.

This paper presents the results from tests of the equivalent bodies of revolution and the minimum drag data obtained from the flight results of rocket-boosted models. Comparisons are made between the original and revised configurations. All tests were conducted at the Langley Pilotless Aircraft Research Station at Wallops Island, Va.

SYMBOLS

A	cross-sectional area, sq ft
a_l/g	longitudinal-accelerometer reading
a_n/g	normal-accelerometer reading
$\bar{c}$	mean aerodynamic chord, ft
C_c	chord-force coefficient, positive in rearward direction, $-\frac{a_l}{g}\frac{W}{qS}$
$C_{D_{tot}}$	total drag coefficient, $C_c \cos \alpha + C_N \sin \alpha$
C_N	normal-force coefficient, positive toward top of model, $\frac{A_n}{g}\frac{W}{qS}$
g	acceleration due to gravity, 32.2 ft/sec^2
H	total pressure, lb/sq ft
l	length, ft
M	Mach number
m/m_o	ratio of total mass flow through ducts to mass flow at free-stream conditions passing through an area equal to total inlet capture area
p	static pressure, lb/sq ft

q	dynamic pressure, lb/sq ft
R	Reynolds number
r	radius, ft
S	total wing area, sq ft
t	time, sec
V	velocity, ft/sec
W	weight, lb
x	station measured from nose, ft
α	angle of attack, deg
γ	flight-path angle, deg, or ratio of specific heats

Subscripts:

b	base
e	duct exit
i	duct inlet (capture)
o	free stream
base	base
ext	external
int	internal
tot	total

MODELS AND APPARATUS

Models

Figure 1 presents a three-view drawing of the original airplane configuration (hereafter called configuration 1) and the revised configuration (hereafter called configuration 2) which shows the differences

between the two designs. Briefly, the primary modifications incorporated on configuration 2 are as follows:

(a) Increased forebody length,

(b) Wing thickness reduced from 7 to 5 percent at the root chord and from 4.5 to 3.2 percent at the tip chord,

(c) Reduced wing fillet thickness,

(d) Modified rear fuselage lines,

(e) Modified pilot's enclosure,

(f) Reduced vertical-tail thickness,

(g) Extension of duct inlets and incorporation of boundary-layer bleeds.

The ratio of maximum normal cross-sectional area to wing area was reduced from 0.0758 to 0.0619. Table I presents the full-scale dimensions of configurations 1 and 2. The rocket models tested in this investigation were 0.10- and 0.125-scale models of configurations 1 and 2, respectively, and photographs of these models are shown as figures 2 and 3.

Both of these models were instrumented to obtain base and internal drag. In order to allow for a minimum of instrumentation, the internal drag was obtained only at Mach numbers above 1.0 by choking the duct at the exit. This was accomplished on the model of configuration 1 by installing a choking cup at the exit as discussed in reference 1. The base of this choking cup was instrumented to obtain the base pressure coefficient of the cup which was used to determine the base drag coefficient. The duct of the model of configuration 2 was choked at supersonic speeds by placing a minimum section at the duct exit and the base drag was obtained from static-pressure measurements made around the base of the model.

In both cases the data necessary to determine internal drag at Mach numbers greater than 1.0 were obtained from measurements made at the choking section. The internal ducting on both models (forward of the choking section) was similar. On each model the two wing root inlets had rounded lips and the ducts merged together to form a common exit through the base.

Figure 4 is a photograph of the model-booster combination of configuration 2. The models were boosted by 6.25-inch-diameter ABL Deacon rocket motors. After the rocket motors had stopped thrusting, the models

separated from their boosters and the data presented herein were obtained during this coasting phase of the flight.

Shown in figures 5 and 6 are the dimensionless area distributions and equivalent bodies of revolution of configurations 1 and 2, respectively. Values of total cross-sectional area used in figures 5 and 6 were corrected for internal flow (mass-flow ratio of 0.70). A part of the data presented herein was obtained with fin-stabilized models which were designed from the equivalent-body plots of figures 5 and 6. A photograph of a typical fin-stabilized equivalent-body model is shown with its push plate in figure 7. These models were flight tested from the helium gun at the Langley Pilotless Aircraft Research Station at Wallops Island, Va.

Apparatus

The helium gun used to test the equivalent body models in flight operates by accelerating the model with its cradle and push plate through a 6-inch-bore barrel by releasing a charge of compressed helium. Once out of the barrel, the cradle and push plate separate and the model is tracked with a CW Doppler radar unit. A photograph of the helium gun is shown in figure 8.

Each of the two rocket models was equipped with an internal telemeter unit which transmits flight data to a ground receiving station where they are recorded. The quantities measured in the two rocket-model tests were angle of attack, longitudinal, normal, and transverse accelerations, and free-stream total pressure. Duct exit static pressure was measured on configuration 1 and duct total pressure and base static pressure were measured on configuration 2.

A rawinsonde released at the time of firing recorded free-stream temperature, static pressure, and winds aloft. The positions of the models in space were determined by an NACA modified radar tracking unit and velocity was determined with the CW Doppler radar unit mentioned previously.

ANALYSIS OF DATA

The drag coefficients of the rocket-boosted models presented herein are based on the total wing area of the models. The total drag coefficients presented represent essentially the minimum drag coefficients of the models since the measured angles of attack were very small for both of the models and the trim normal-force coefficient was never greater than ± 0.03.

Since the velocity of the models was also determined from the CW Doppler radar set, another source of total drag data was available as well as that obtained from the telemeter values. This method of obtaining total drag consisted of differentiating the velocity with respect to time, correcting for flight-path angle, and calculating the total drag coefficient by the relationship

$$C_{D_{tot}} = -\left(\frac{dv}{dt} + g \sin \gamma\right)\frac{W}{qSg}$$

Reference 2 discusses the CW Doppler radar set and its method of determining velocity in more detail.

In order to present the external drag coefficient of the models $\left(C_{D_{ext}} = C_{D_{tot}} - C_{D_{int}} - C_{D_{base}}\right)$, it was necessary to determine the internal and base drag in each case. The internal drag was calculated by the method of reference 3. This method consists essentially of determining the loss in total momentum of air flowing through the duct between free stream and exit. The equation used for computing the internal drag coefficient is as follows:

$$C_{D_{int}} = \frac{2A_e}{S}\left[\frac{m}{m_o}\left(\frac{A_i}{A_e}\right) - \frac{p_e}{p_o}\left(\frac{M_e}{M_o}\right)^2 - \left(\frac{p_e - p_o}{\gamma p_o M_o{}^2}\right)\right]$$

This coefficient could only be determined in these tests for Mach numbers greater than 1.0, since at lower Mach numbers the duct was unchoked and all the data needed to satisfy the above equation could not be obtained.

Base drag of the rocket models was calculated by the following equation:

$$C_{D_{base}} = \frac{-(p_b - p_o)(\text{base area})}{qS}$$

In the case of configuration 1, the only base drag coefficients determined were for the choking cup since the base of the model itself closely duplicated that of the full-scale airplane. In the case of configuration 2, the base drag was determined over the entire solid portion of the base annulus.

The tests of small fin-stabilized bodies of revolution provide a simple and inexpensive means of obtaining zero-lift pressure drag and drag-rise Mach number data of thin, low-aspect-ratio wing-body combinations. During the flight of such models, the velocity is obtained by means of the CW Doppler radar set and the drag is determined by the same method as discussed previously in relation to the rocket-model tests.

ACCURACY

A table showing the accuracy of the various coefficients and data presented from these tests is presented. Wherever possible, these values have been determined on the basis of comparisons between several sources of data but, where this was not possible, the accuracy has been estimated on the basis of the maximum probable instrument error.

	Rocket-model configuration 1		Rocket-model configuration 2		Equivalent bodies of revolution
	M = 0.80	M = 1.35	M = 0.93	M = 1.27	M = 1.15
M	±0.010	±0.005	±0.010	±0.005	±0.01
$C_{D_{tot}}$ . .	0.001	0.001	0.001	0.002	±0.001
$C_{D_{base}}$ . .	±0.0002	±0.0001	±0.0002	±0.0001	------
$C_{D_{int}}$ . .	-------	±0.0001	-------	±0.0003	------

RESULTS AND DISCUSSION

Figure 9 presents the variation of Reynolds number with Mach number for the tests reported herein and are based on the length of the wing mean aerodynamic chord.

Mass-Flow Ratio

The variation of the mass-flow ratio m/m_o with Mach number M for the two rocket models is shown in figure 10. The model of configuration 1 operated at about a constant value of 0.62 from M = 1.00 to M = 1.34. Mass-flow ratios for configuration 2 varied from 0.88 at M = 1.04 to 1.00 at M = 1.64.

Although the two models were tested at different values of m/m_o, this does not invalidate a comparison of external drag since in both cases the values of m/m_o for the model tests were selected to duplicate the engine requirements at a reasonable Mach number and altitude. The difference between the two curves shown in figure 10 is the result of the different operating requirements of the two different assumed engines used in airplane configurations 1 and 2. As long as m/m_o for the rocket models duplicates that of the full-scale airplane, the spillage drag (and therefore the external drag) will duplicate that of the full-scale airplane.

Total-Pressure Recovery

Figure 11 presents values of duct total-pressure recovery for configuration 2. These values are to be considered qualitative since they were measured near the duct exit. They therefore represent the loss in total pressure between free-stream conditions and the duct exit rather than at the engine face. The losses between the engine face and the exit, however, are believed to be small.

Drag

Drag estimates discussed more completely in reference 1 indicated large drag reductions could be obtained at supersonic speeds by redesign of the sharply boattailed afterbody and reduction in wing-fillet frontal area. These estimates were extended to include possible drag reduction by modification of other components listed in a previous section. The summation of the various estimated reductions indicated a $C_{D_{ext}}$ value of 0.022 at $M = 1.5$. There were no interference effects considered in the calculation of this value.

Because of the large drag reduction indicated by the estimate made at $M = 1.5$, further tests were made with equivalent bodies of revolution of configurations 1 and 2. The results of these tests are shown in figures 12 and 13. Figure 12 presents the total drag coefficient of each of the two configurations based on maximum cross-sectional equivalent body area.

The drag increments due to zero lift pressure drag ΔC_D as obtained from figure 12 are shown based on wing area in figure 13. The curve of configuration 1 shows a maximum ΔC_D of 0.027 at $M = 1.08$. Configuration 2 shows ΔC_D to be approximately 0.016 between $M = 1.10$ and $M = 1.24$. This indicates a reduction in ΔC_D of 0.011 when compared with the equivalent body of revolution of configuration 1. Another significant improvement shown by the equivalent model of configuration 2

was that the drag rise was delayed about 0.04 in Mach number. Throughout this paper the drag-rise Mach number is defined as the Mach number at which $\frac{dC_D}{dM} = 0.10$.

After the results of the tests of the equivalent bodies of revolution had been examined, it was decided to test a large-scale rocket drag model of configuration 2. The total drag coefficient $C_{D_{tot}}$ obtained from this test is shown in figure 14. During a portion of the flight, it was possible to obtain $C_{D_{tot}}$ from the CW Doppler radar unit as well as from the quantities obtained from the telemeter. These values are presented for comparison in figure 14 and show excellent agreement through the transonic and low supersonic Mach number range where comparisons are possible.

Figure 15 presents the base and internal drag coefficients for the model of configuration 2. As mentioned previously, the internal drag coefficient $C_{D_{int}}$ could not be determined at Mach numbers less than 1.0. The values of $C_{D_{int}}$ were small and had a maximum value of 0.001 at $M = 1.64$. At Mach numbers near 1.0, $C_{D_{int}}$ is very close to zero.

The external drag coefficient $C_{D_{ext}}$ from the test of configuration 2 is presented in figure 16. Also shown for purposes of comparison are the results of configuration 1 (from ref. 1). It should be pointed out that the $C_{D_{ext}}$ values of configuration 1 were corrected for the same increment of internal drag (about 0.0008) at subsonic speeds as at supersonic speeds. This assumption at subsonic speeds is not made on configuration 2 because of the trend of the $C_{D_{int}}$ values shown in figure 15.

Configuration 2 resulted in a delay in drag rise Mach number from 0.93 to 0.97 and a reduction in $C_{D_{ext}}$ from 0.038 to 0.024 at $M = 1.35$. The overall decrease in $C_{D_{ext}}$ was in good agreement with estimated reductions and results from the equivalent body tests in figure 13.

CONCLUSIONS

The results of an investigation to determine the reduction in minimum drag at supersonic speeds resulting from the redesign of various components of a proposed airplane indicate the following conclusions:

1. There is a decrease in external drag coefficient at a Mach number of 1.00 from 0.035 to 0.022. Between Mach numbers of 1.00 and 1.35, there is an average reduction of about 0.013 and at a Mach number of 1.35, the external drag coefficient is reduced from 0.038 to 0.024.

2. The drag-rise Mach number is delayed from 0.93 to 0.97.

3. The fin-stabilized equivalent bodies predicted the transonic pressure drag increment and drag-rise Mach number very accurately in these tests.

Langley Aeronautical Laboratory,
National Advisory Committee for Aeronautics,
Langley Field, Va., April 20, 1956.

REFERENCES

1. Mitcham, Grady L., and Blanchard, Willard S., Jr.: Low-Lift Drag and Stability Data From Rocket Models of a Modified-Delta-Wing Airplane With and Without External Stores at Mach Numbers From 0.8 to 1.36. NACA RM L53A27, 1953.

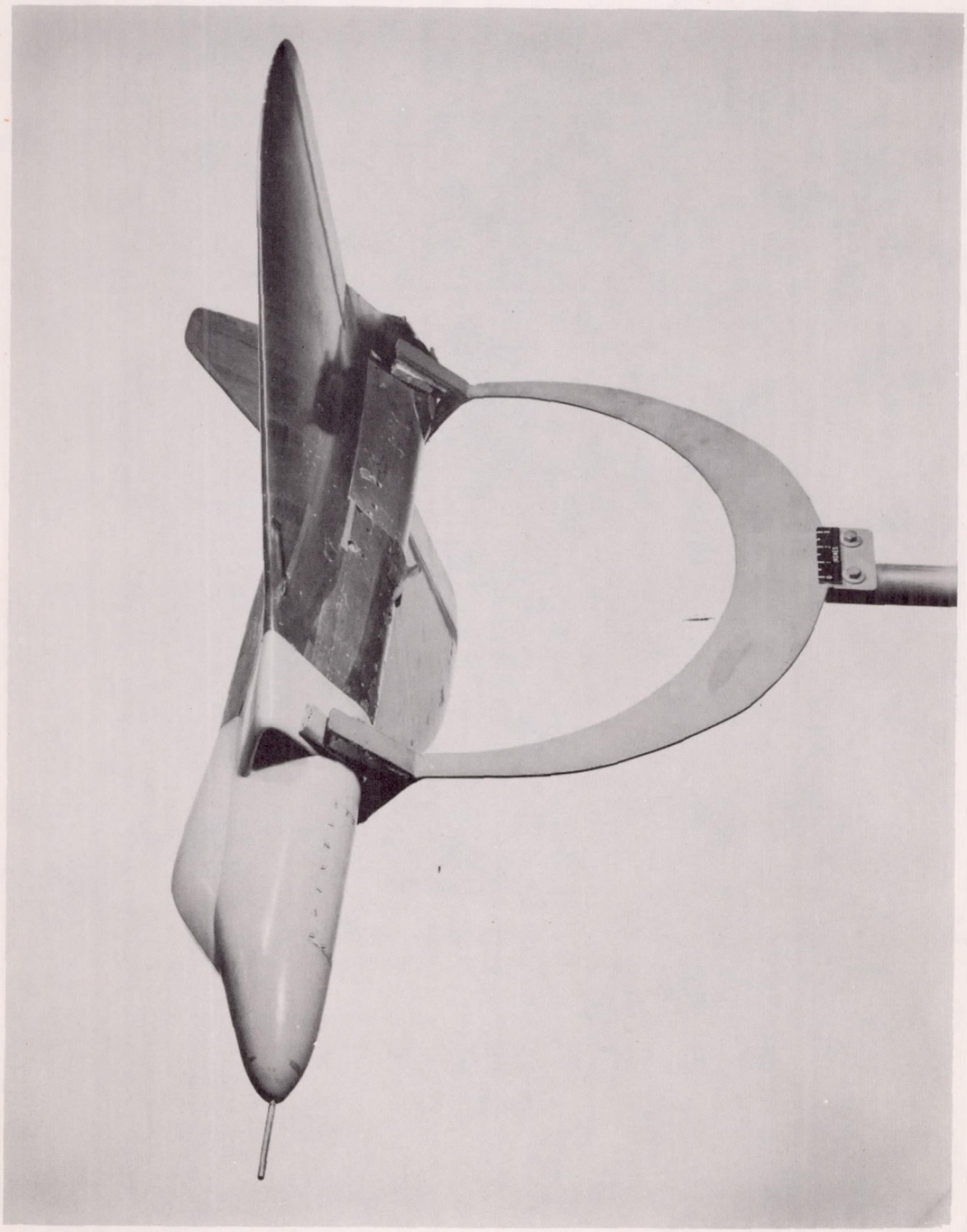
2. Wallskog, Harvey A., and Hart, Roger G.: Investigation of the Drag of Blunt-Nosed Bodies of Revolution in Free Flight at Mach Numbers From 0.6 to 2.3. NACA RM L53D14a, 1953.

3. Faget, Maxime A., Watson, Raymond S., and Bartlett, Walter A., Jr.: Free-Jet Tests of a 6.5-Inch-Diameter Ram-Jet Engine at Mach Numbers of 1.81 and 2.00. NACA RM L50L06, 1951.

TABLE I.- PHYSICAL CHARACTERISTICS OF TWO VERSIONS OF A FULL-SCALE MODIFIED DELTA-WING AIRPLANE

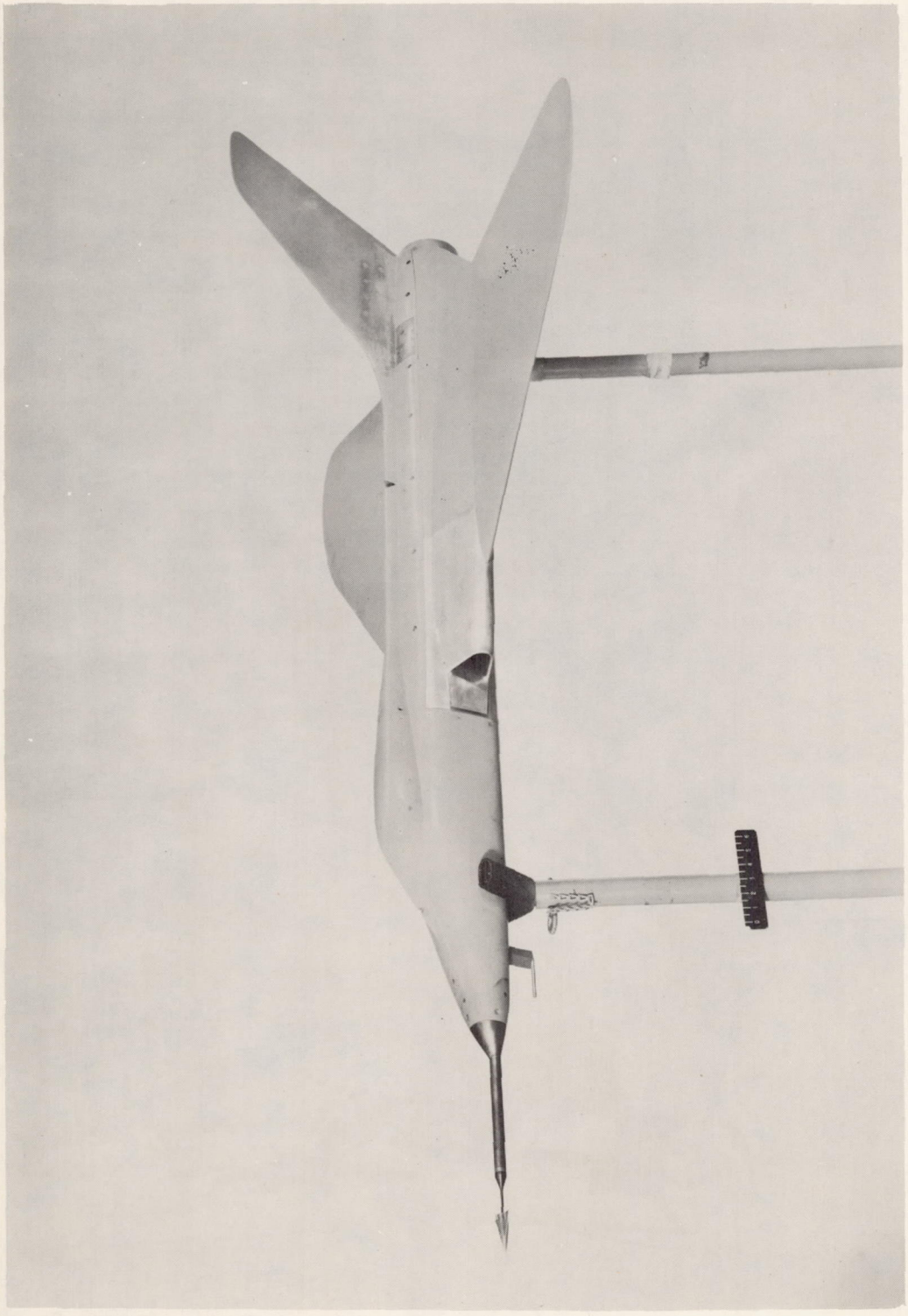
	Configuration 1	Configuration 2
Wing:		
Area (total), sq ft	557	557
Span, ft	33.5	33.5
Aspect ratio	2.01	2.01
Mean aerodynamic chord, ft	18.2	18.2
Airfoil section at root	NACA 0007 (modified)	NACA 0005 (modified)
Airfoil section at tip	NACA 0004.5 (modified)	NACA 0003.2 (modified)
Taper ratio	0.33	0.33
Sweepback of leading edge, deg	52.5	52.5
Dihedral (relative to mean thickness line)	0	0
Vertical tail:		
Height (above fuselage reference plane), ft	10.0	11.8
Tip chord, ft	3.2	4.7
Airfoil section at tip	NACA 0006 (modified)	NACA 0003.2 (modified)
Airfoil section at a water line 28.5 inches above fuselage reference plane	NACA 0008 (modified)	NACA 0005 (modified)
Area (above a water line 28.5 inches above fuselage reference plane), sq ft	47.7	69.9
Duct inlet capture area, sq ft	4.2	4.2

Figure 1.- Three-view drawing of configurations 1 and 2.



L-71188

Figure 2.- Photograph of configuration 1.



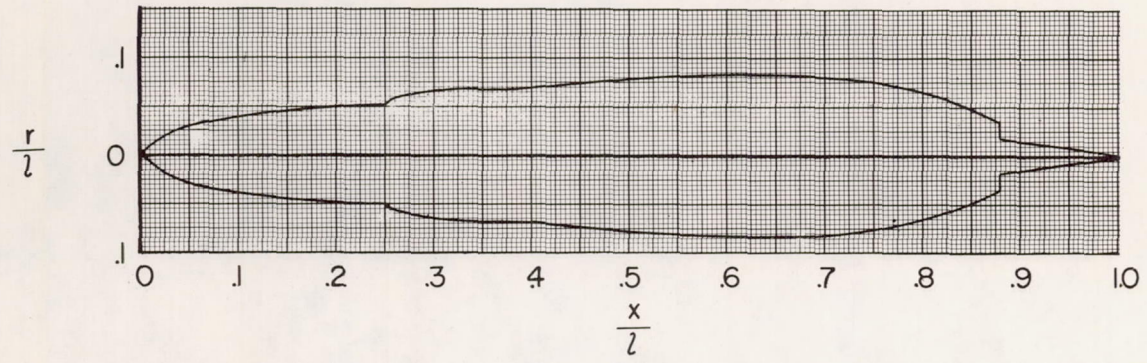
L-91964.1

Figure 3.- Photograph of configuration 2.

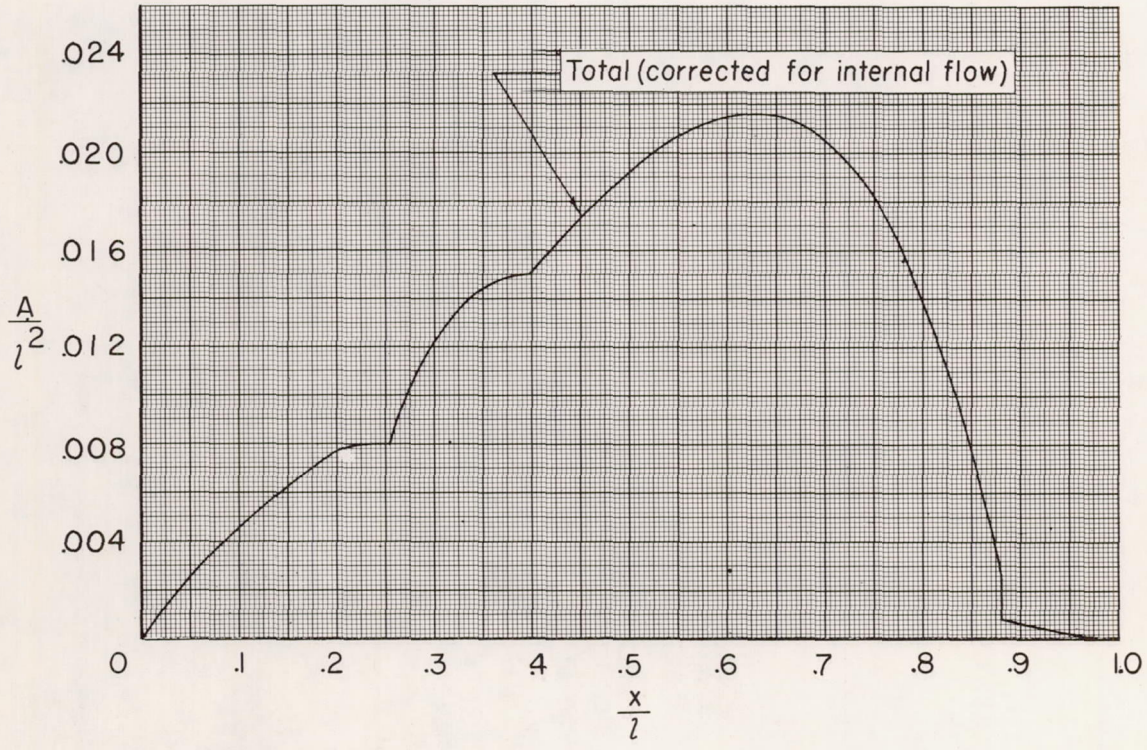


L-92182.1

Figure 4.- Photograph of configuration 2 on booster prior to launching.

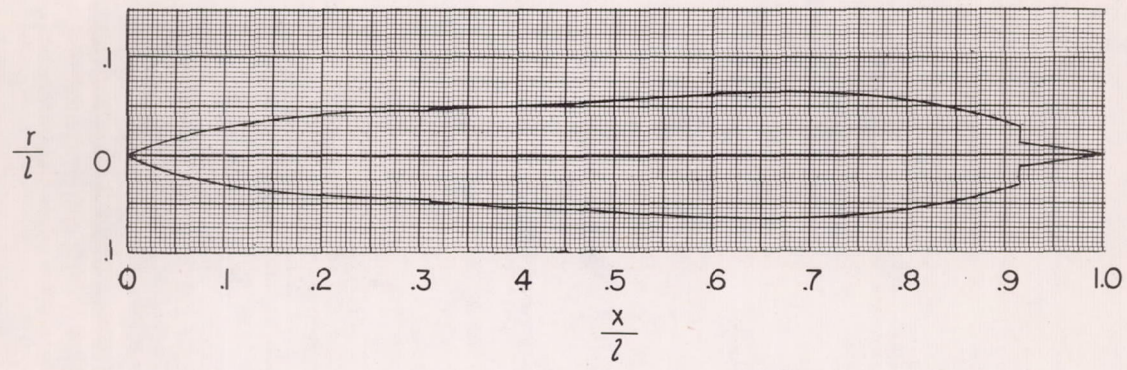


(a) Equivalent body of revolution.

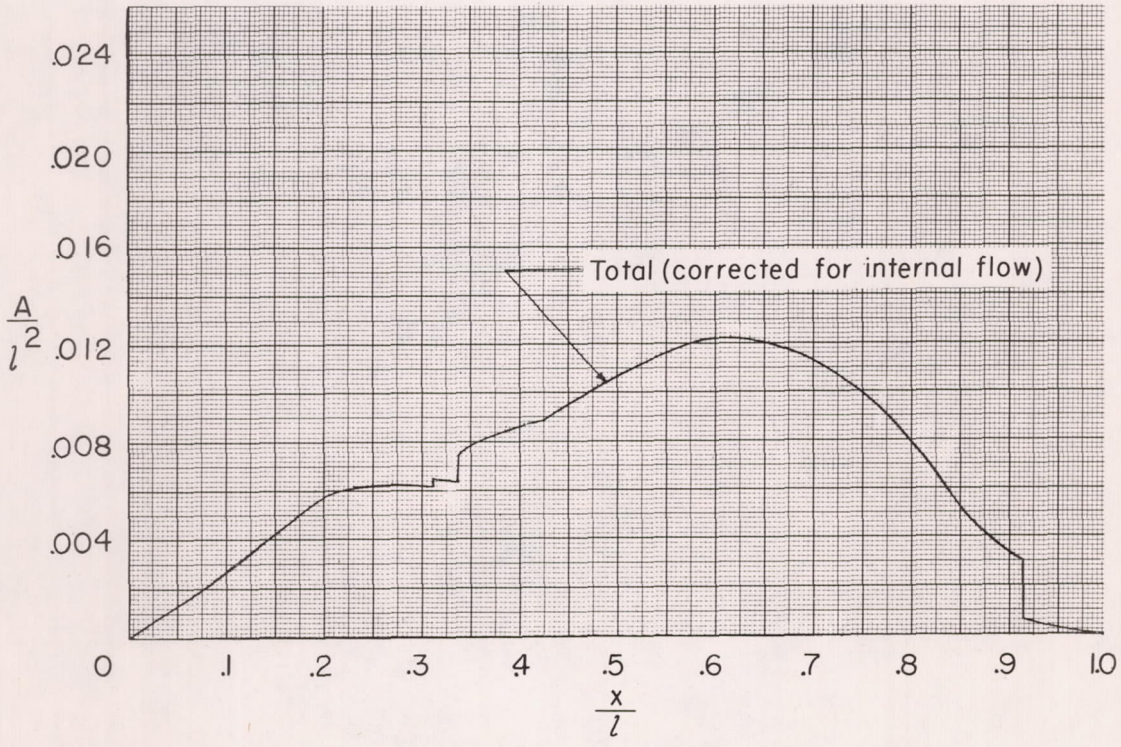


(b) Area distribution.

Figure 5.- Equivalent body of revolution and cross-sectional area distribution of configuration 1.

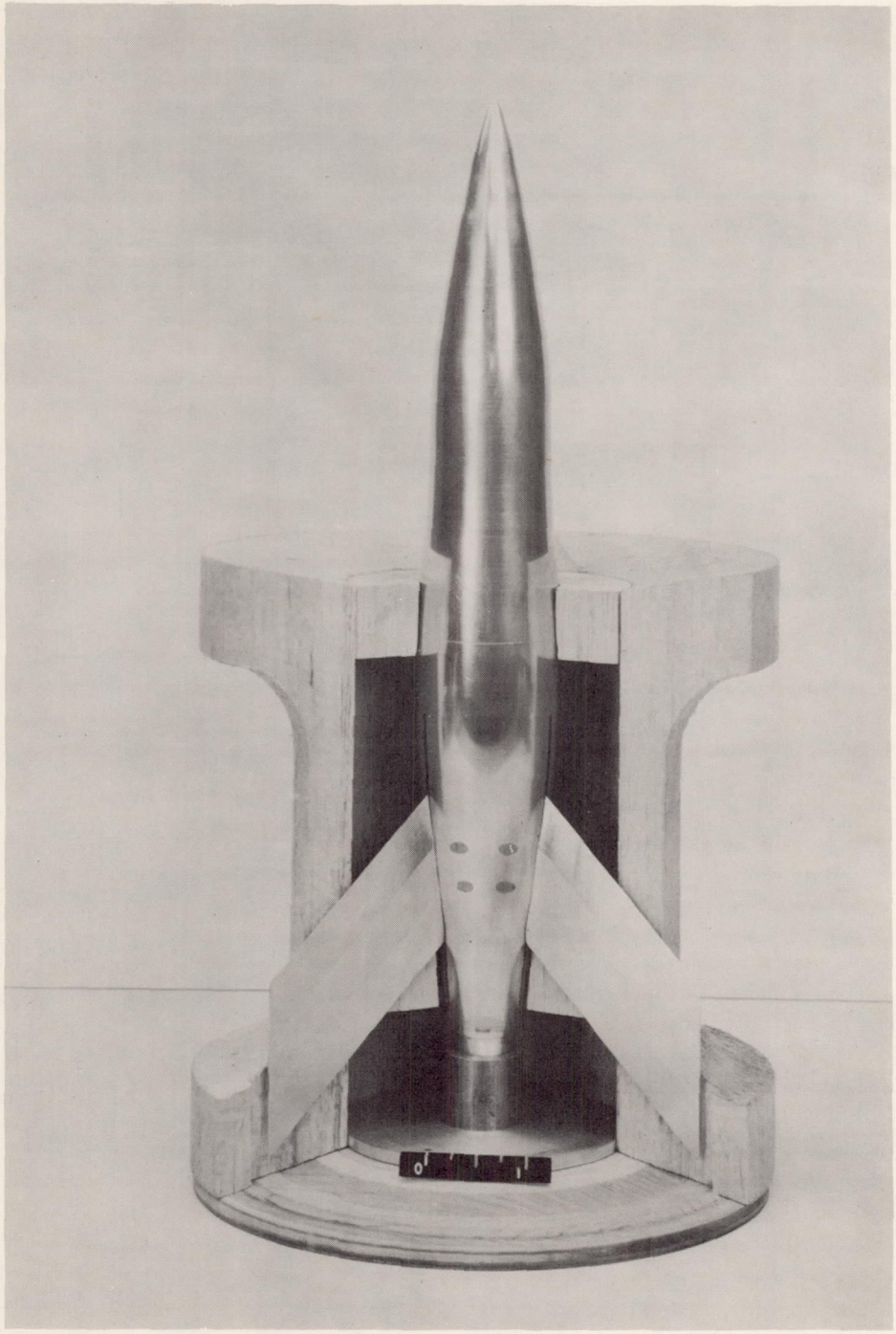


(a) Equivalent body of revolution.



(b) Area distribution.

Figure 6.- Equivalent body of revolution and cross-sectional area distribution of configuration 2.



L-79811

Figure 7.- Cutaway photograph of typical equivalent body of revolution model mounted in cradle.

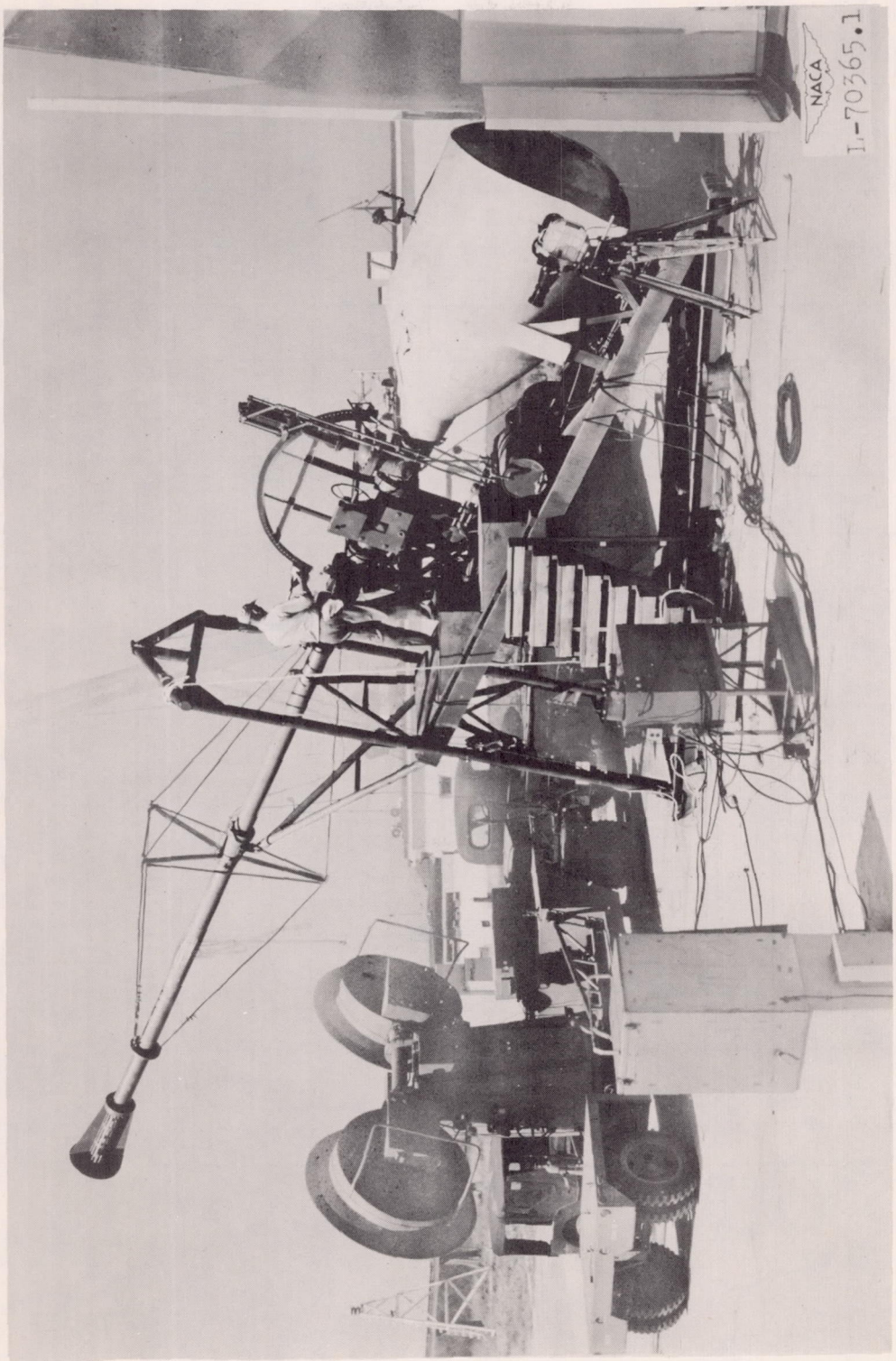


Figure 8.- Photograph of helium gun.

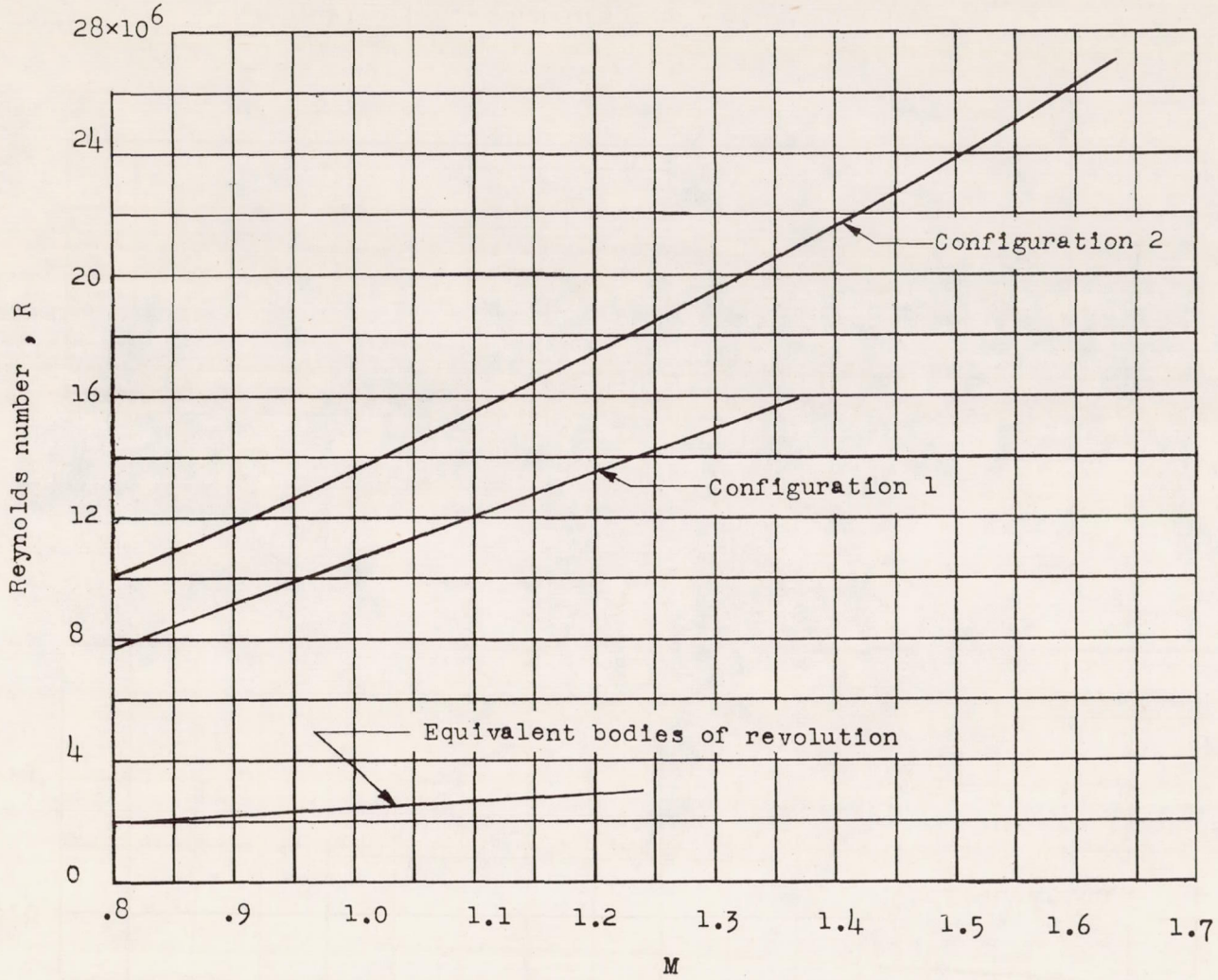


Figure 9.- Reynolds number ranges for the tests (based on the length of the mean aerodynamic chord).

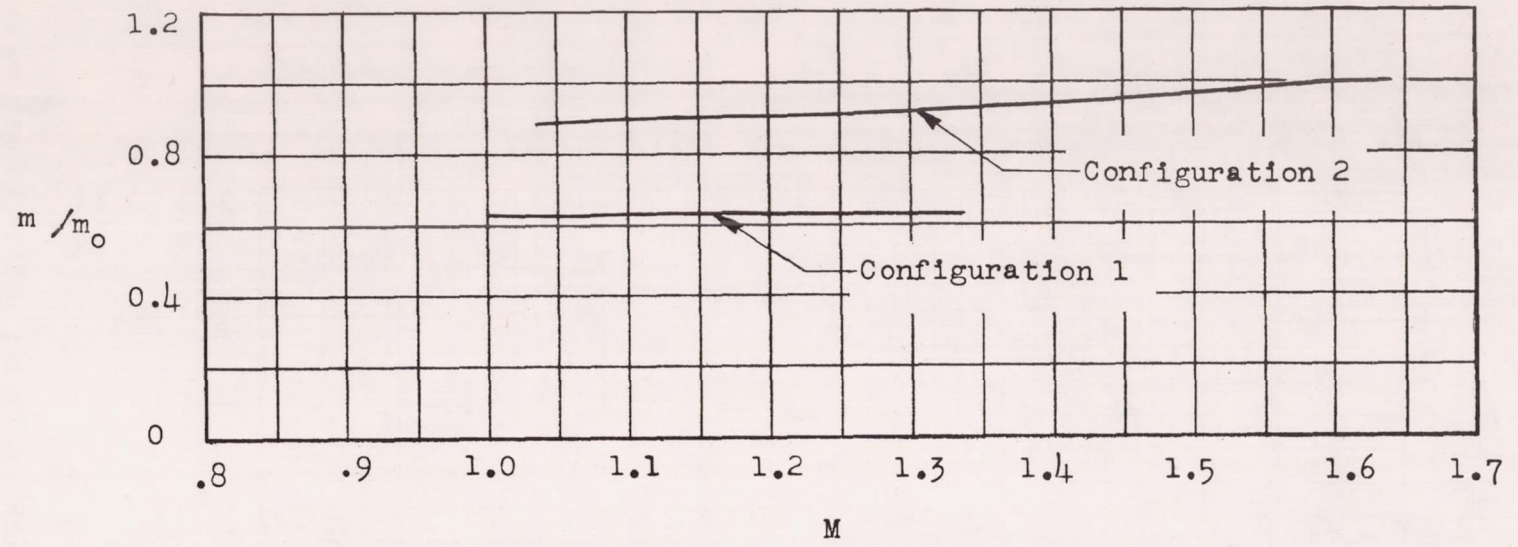


Figure 10.- Mass-flow ratio.

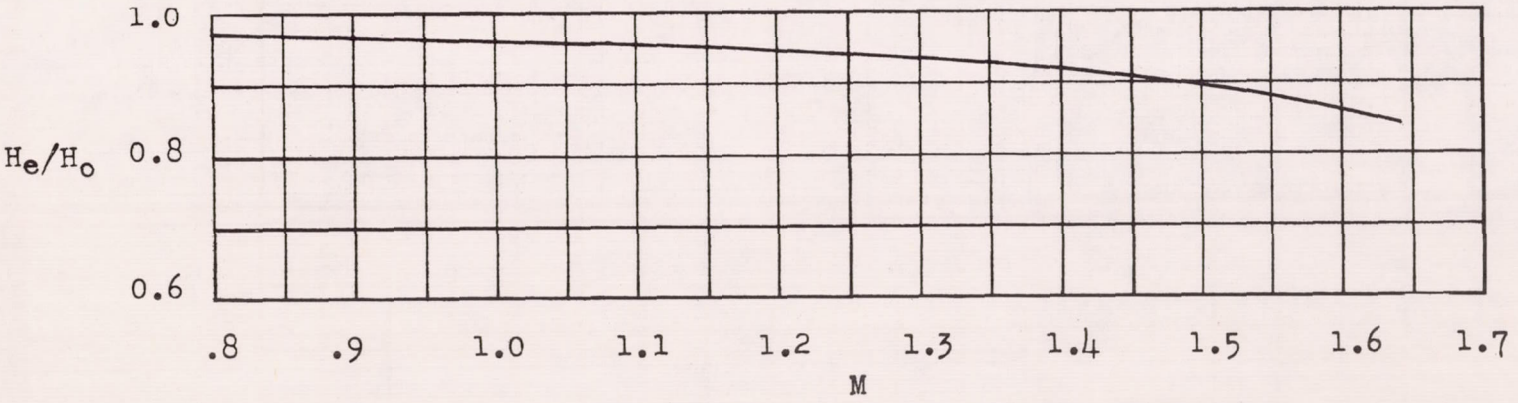


Figure 11.- Total-pressure recovery of configuration 2.

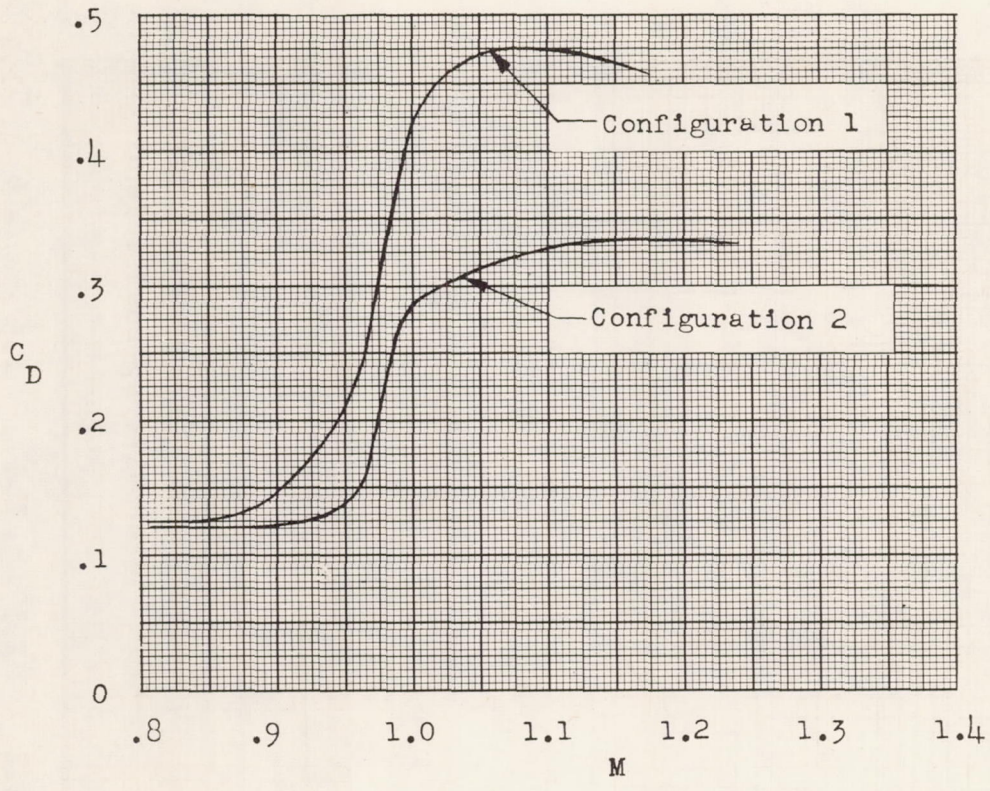


Figure 12.- Drag coefficient of equivalent bodies (based on maximum cross-sectional area).

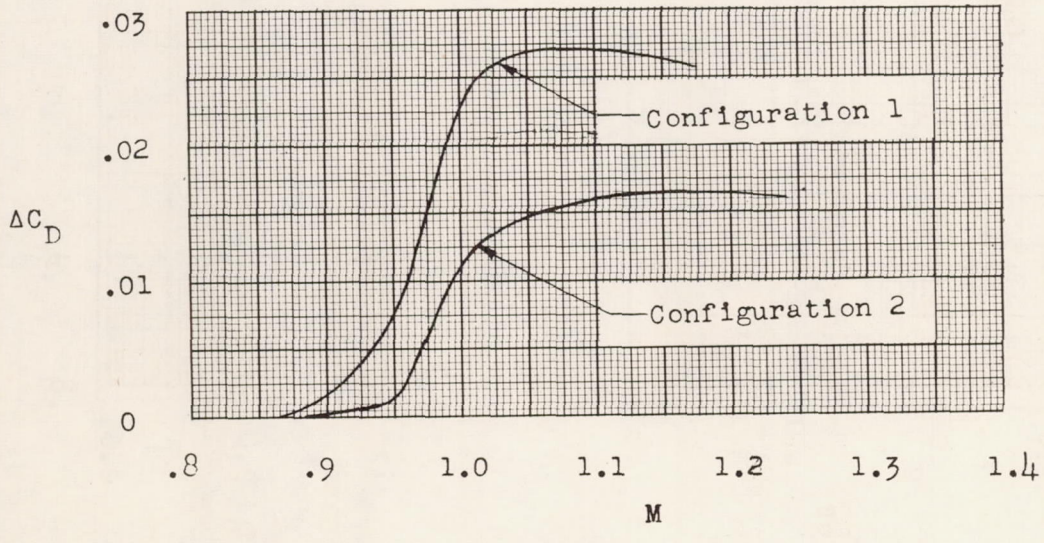


Figure 13.- Drag-rise coefficient from equivalent bodies (based on wing area).

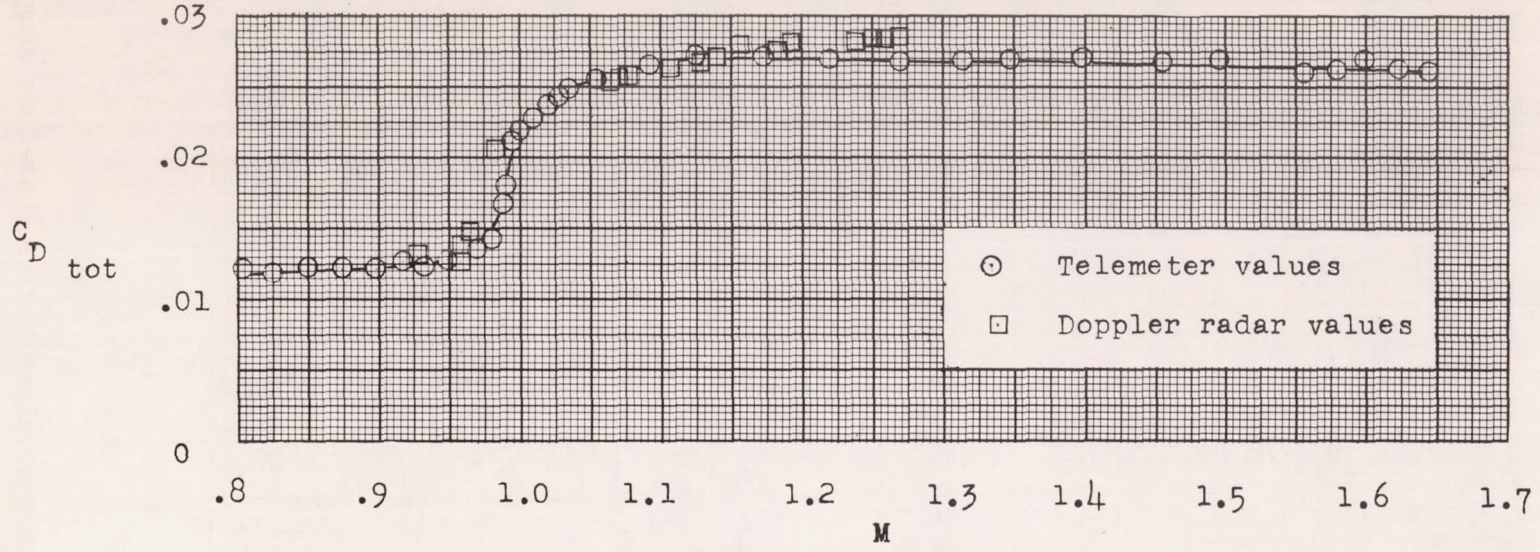


Figure 14.- Total drag coefficient of configuration 2.

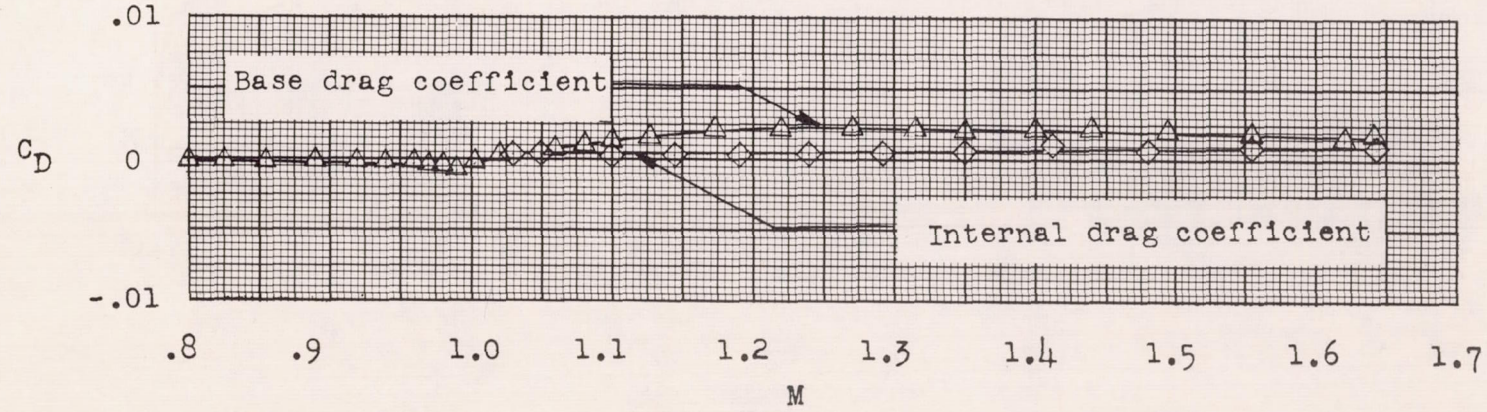


Figure 15.- Base and internal drag coefficients of configuration 2.

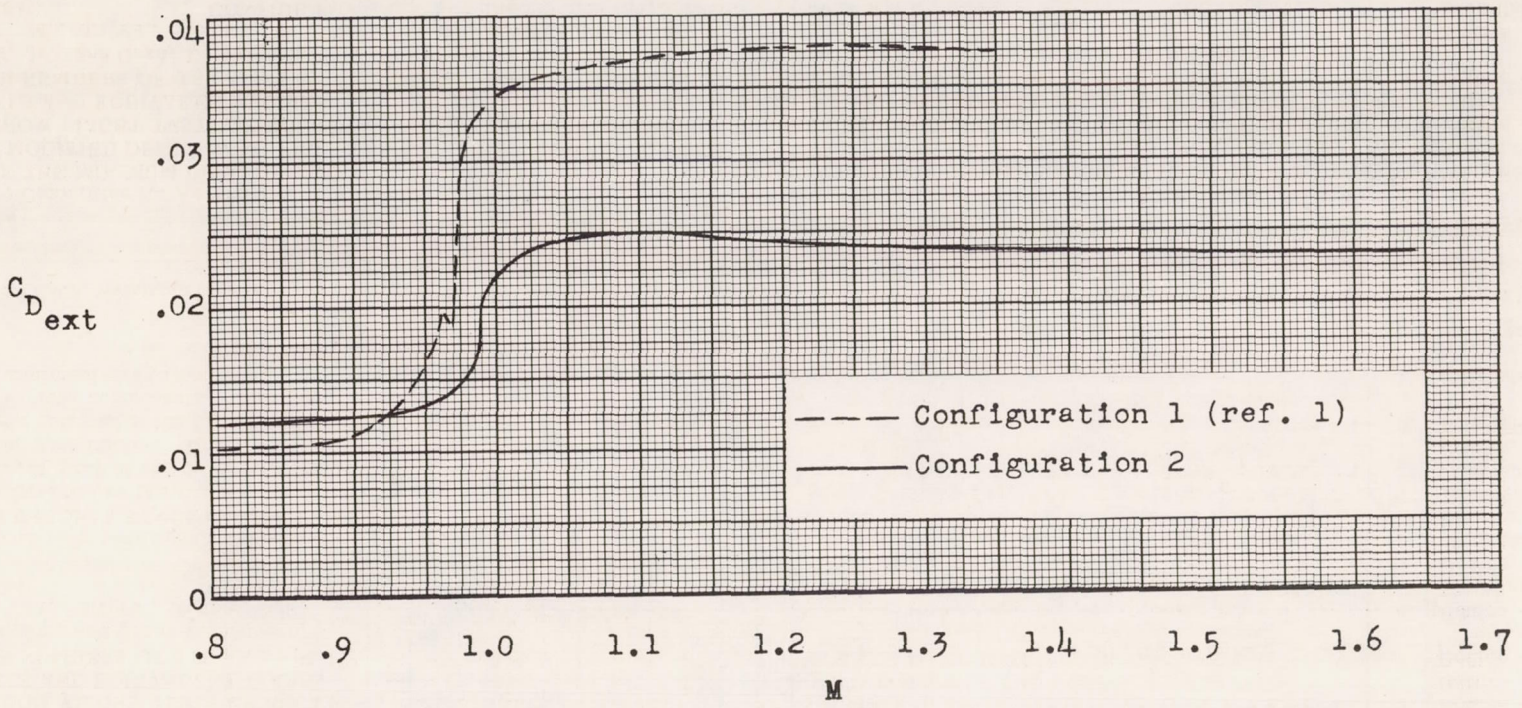


Figure 16.- External drag coefficients of configurations 1 and 2.